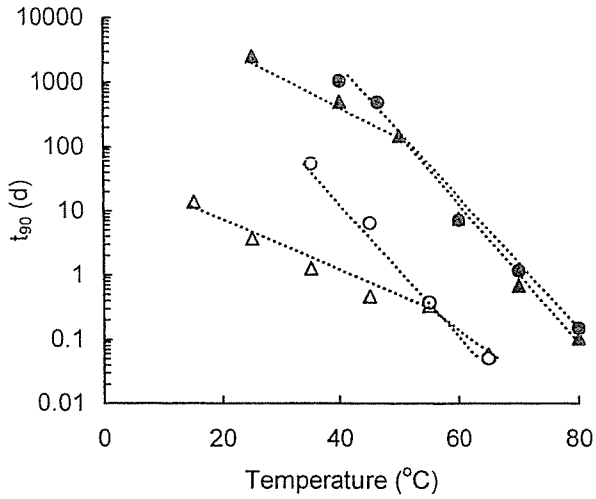

Figure 7. Temperature dependence of t_{90} for nifedipine–PVP (9:1 w/w) solid dispersions (▲), amorphous nifedipine (△), phenobarbital–PVP (95:5 w/w) solid dispersions (●), and amorphous phenobarbital (○).

for pure amorphous nifedipine (49°C) or phenobarbital (45°C).[23]

Stabilization by addition of a small amount of PVP has previously been reported for indomethacin–PVP and sucrose–PVP solid dispersions.[9–13] It has been reported that enthalpy relaxation of sucrose becomes slower when colyophilized with dextran, PVP, poly(vinylpyrrolidon-*co*-vinylacetate), or trehalose, even at a temperature at which the difference between T_g and storage temperature ($T_g - T$) is similar. This result indicates that the mobility of sucrose is reduced in the presence of the additives at temperature $<T_g$.[24]

Proportion of glass that has relaxed after storage at 25°C for nifedipine– and phenobarbital–PVP solid dispersions are shown in Figure 8. The previously reported[23] time profiles for the pure amorphous drugs are also shown. Enthalpy relaxation time (τ_e) of amorphous nifedipine, estimated according to the Kohlraush–Williams–Watts equation (eq. 12), increased from 1.2 to 18 days in the presence of 10% PVP, and the τ_e of amorphous phenobarbital increased from 1.0 to 3.7 days in the presence of 5% PVP.

$$\phi(t) = 1 - \frac{\Delta H_t}{\Delta H_\infty} = \exp\{-(t/\tau_e)^\beta\} \qquad (12)$$

where ΔH_t is the enthalpy recovered after storage for time t, β is a parameter that describes the distribution of relaxation time, and ΔH_∞ is the enthalpy change necessary for a glass to relax to a

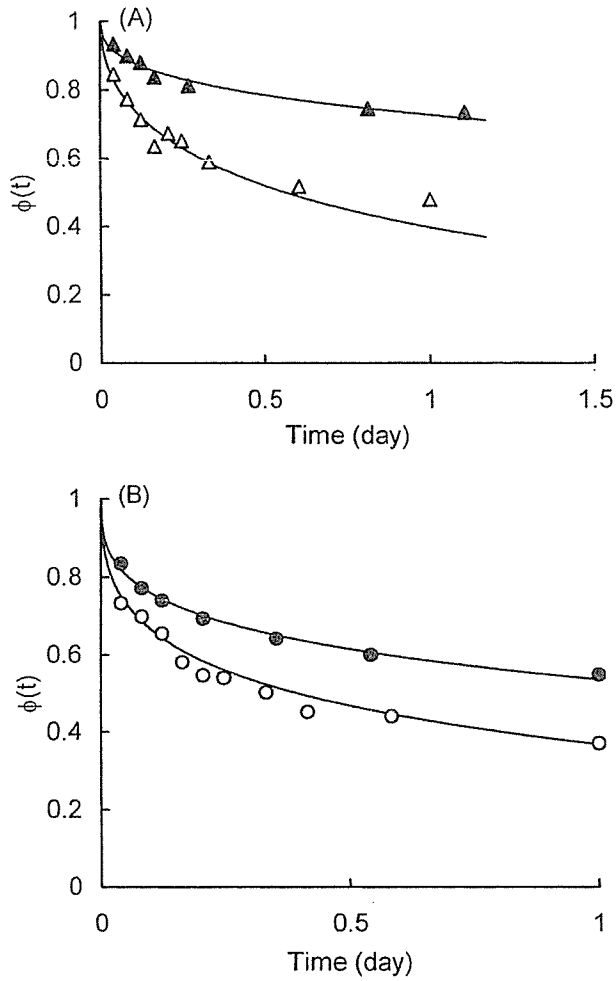

Figure 8. Proportion of glass that has relaxed for (A) nifedipine and (B) phenobarbital after storage at 25°C. Key: (△) nifedipine in the absence of PVP; (▲) nifedipine in the presence of PVP; (○) phenobarbital in the absence of PVP; and (●) phenobarbital in the presence of PVP. Solid lines were generated by fitting the data to the Kohlraush–Williams–Watts equation.

supercooled liquid. ΔH_∞ is calculated according to eq. 13[24]:

$$\Delta H_\infty = \Delta C_{p,Tg}(T_g - T) \qquad (13)$$

where ΔC_p is the change in the heat capacity at T_g, and T is storage temperature.

Although the increase in enthalpy relaxation time by addition of PVP was small compared with the increase in t_{90}, the stabilization of nifedipine and phenobarbital by a small amount of PVP may partly be attributable to the reduced molecular mobility.

Comparison of the Temperature Dependence of t_{90} and Relaxation Time

The crystallization rate, k, of an amorphous solid at temperature T depends on the rate of molecular diffusion across the nuclear–amorphous matrix interface [$D(T)$] and the nucleation free energy term [$f(T)$], according to eq. 1.[3–6] If the temperature dependence of $D(T)$ is much larger than that of $f(T)$, then t_{90} will be correlated with the mean relaxation time (τ) of the amorphous matrix as shown in eq. 14[1,7]:

$$t_{90}(T_g)/t_{90} \cong k/k(T_g) \cong D_T/D_{Tg} \cong (T/\eta)/[T_g/\eta(T_g)] \cong (T/\tau)/[T_g/\tau(T_g)] \quad (14)$$

where D_T and D_{Tg} are the diffusion coefficients at temperatures T and T_g, respectively.

The τ values for the solid dispersions were calculated according to the AGV equation, by the method previously reported by Zografi et al.[20,21] Because all degrees of freedom of motion contribute to the relaxation of amorphous materials, the mean relaxation time calculated according to the AGV equation has a distribution of relaxation mode that is reflected by the term β of the Kohlraush–Williams–Watts stretched exponential function. The heating rate dependence of the T_g values for the nifedipine–PVP solid dispersion is shown in Figure 9. The fragility of the solid dispersion was calculated from the slope of the line. The D and T_0 values of the AGV equation were calculated from the fragility obtained. The D value for the solid dispersion was estimated to be 15, which is similar to the value for pure amorphous nifedipine(14).[7] This similarity suggests that pure PVP may be as fragile as pure amorphous nifedipine.

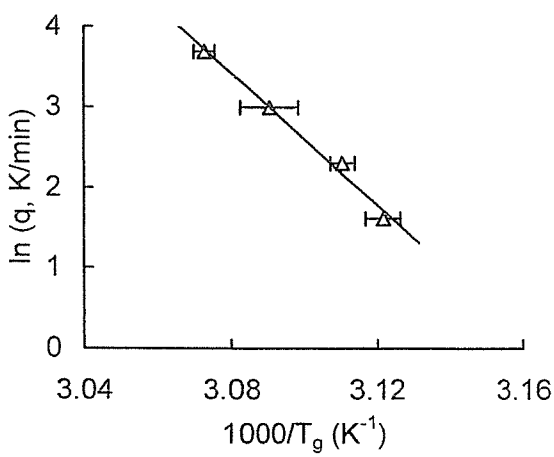

Figure 9. Heating rate (q) dependence of T_g for nifedipine–PVP (9:1 w/w) solid dispersions.

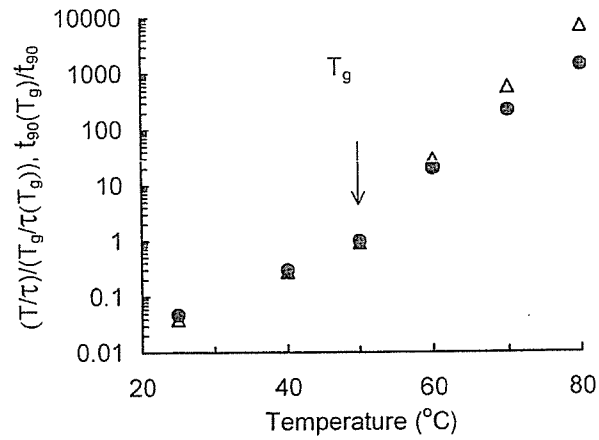

Figure 10. Temperature dependence of (△) $(T/\tau)/[T_g/\tau(T_g)]$ and (●) $t_{90}(T_g)/t_{90}$ for nifedipine–PVP (9:1 w/w) solid dispersions.

The parameters $(T/\tau)/[T_g/\tau(T_g)]$ and $t_{90}(T_g)/t_{90}$ are shown in Figure 10 as a function of temperature. The temperature dependence of $t_{90}(T_g)/t_{90}$ for the nifedipine–PVP solid dispersion seems coincident with that of $(T/\tau)/[T_g/\tau(T_g)]$ in the temperature range $<T_g$, within experimental error, albeit the temperature range studied was small. This result suggests that the temperature dependence of molecular motion [$D(T)$] is much larger than that of $f(T)$ at temperatures $<T_g$ in the presence of PVP. In other words, the free energy barrier for the molecular motion may be larger than that for the nuclei formation of amorphous nifedipine in the solid dispersion at temperatures $<T_g$, as reported for amorphous indomethacin crystallization.[25]

To predict the crystallization rate of amorphous drugs precisely, the temperature dependence of both the molecular mobility and the activation free energy of nuclei formation should be known. In practical purposes, however, the approximate t_{90} value of overall crystallization at temperatures $<T_g$ can be estimated from the information on the temperature dependence of molecular mobility and crystallization rate at temperatures around T_g.

REFERENCES

1. Guo Y, Byrn S, Zografi G. 2000. Physical characteristics and chemical degradation of amorphous

quinapril hydrochloride. J Pharm Sci 89:128–143.
2. Shamblin SL, Tang X, Chang L, Hancock BC, Pikal MJ. 1999. Characterization of the time scales of molecular motion in pharmaceutically important glasses. J Phys Chem B 103:4113–4121.
3. Hancock BC, Zografi G. 1997. Characteristics and significance of the amorphous state in pharmaceutical systems. J Pharm Sci 86:1–12.
4. Ngai KL, Magill JH, Plazek DJ. 2000. Flow, diffusion and crystallization of supercooled liquid: Revisited. J Chem Phys 112:1887–1892.
5. Saleki-Gerhardt A, Zografi G. 1994. Non-isothermal and isothermal crystallization of sucrose from the amorphous state. Pharm Res 11:1166–1173.
6. Rodriguez-Hornedo N, Murphy D. 1999. Significance of controlling crystallization mechanism and kinetics in pharmaceutical systems. J Pharm Sci 88:651–660.
7. Aso Y, Yoshioka S, Kojima S. 2001. Explanation of the crystallization rate of amorphous nifedipine and phenobarbital from their molecular mobility as measured by ^{13}C NMR relaxation time and the relaxation time obtained from the heating rate dependence of T_g. J Pharm Sci 89:128–143.
8. Hodge IM. 1987. Effects of annealing and prior history on enthalpy relaxation in glassy polymers. 6. Adam-Gibbs formulation of nonlinearity. Macromolecules 20:2897–2908.
9. Yoshioka M, Hancock BC, Zografi G. 1995. Inhibition of indomethacin crystallization in Poly(vinylpyrrolidone) coprecipitate. J Pharm Sci 84:983–986.
10. Matsumoto T, Zografi G. 1999. Physical properties of solid molecular dispersions of indomethacin with poly(vinylpyrrolidone) and poly(vinyl pyrrolidone-co-vinyl-acetate) in relation to indomethacin crystallization. Pharm Res 16:1722–1728.
11. Shamblin SL, Zografi G. 1999. The effect of absorbed water on the properties of amorphous mixtures containing sucrose. Pharm Res 16:1119–1124.
12. Zeng XM, Martin GP, Marriott C. 2000. Effects of molecular weight of polyvinylpyrrolidone on the glass transition temperature and crystallization of co-lyophilized sucrose. Int J Pharm 218:63–73.
13. Taylor LS, Zografi G. 1997. Spectroscopic characterization of interactions between PVP and indomethacin in amorphous molecular dispersions. Pharm Res 14:1691–1698.
14. Khougaz K, Clas S. 2000. Crystallization inhibition in solid dispersions of MK-0591 and poly(vinylpyrrolidone) polymer. J Pharm Sci 89:1325–1334.
15. Takeuchi H, Yasuji T, Yamamoto H, Kawashima Y. 2000. Temperature- and moisture-induced crystallization of amorphous lactose on composite particles with sodium alginate prepared by spray-drying. Pharm Dev Technol 5:355–363.
16. Hirayama F, Wang Z, Uekama K. 1994. Effect of 2-hydroxy-β-cyclodextrin on crystllization and polymorphic transition of nifedipine in solid state. Pharm Res 11:1766–1770.
17. Uekama K, Ikegami K, Wang Z, Horiuchi Y, Hirayama F. 1992. Inhibitory effect of 2-hydroxypropyl-β-cyclodextrin on crystal-growth of nifedipine during storage: superior dissolution and oral bioavailability compared with polyvinylpyrrolidone K-30. J Pharm Pharmacol 44:73–78.
18. Kato Y, Watanabe F. 1978. Relationship between polymorphism and bioavailability of phenobarbital. Yakugaku Zasshi 98:639–648.
19. Putnam RL, Boerio-Goates J. 1993. Heat-capacity measurements and thermodynamic functions of crystalline sucrose at temperatures from 5 K to 342 K. Revised values for $\Delta_f G^\circ_m$ (sucrose, cr, 298.15 K), $\Delta_f G^\circ_m$ (sucrose, aq, 298.15 K), S°_m (sucrose. aq, 298.15 K); and $\Delta_r G^\circ_m$ (298.15 K) for hydrolysis of aqueous sucrose. J Chem Thermodyn 25:607–613.
20. Andronis V, Zografi G. 1998. The molecular mobility of supercooled amorphous indomethacin as a function of temperature and relative humidity. Pharm Res 15:835–842.
21. Tong P, Zografi G. 1999. Solid-state characteristics of amorphous sodium indomethacin relative to its free acid. Pharm Res 16:1186–1192.
22. Guinot S, Leveiller F. 1999. The use of MTDSC to assess the amorphous phase content of micronised drug substance. Int J Pharm 192:63–75.
23. Aso Y, Yoshioka S, Kojima S. 2000. Relationship between the crystallization rates of amorphous nifedipine, phenobarbital, and flopropione, and their molecular mobility as measured by their enthalpy relaxation and ^1H NMR relaxation times. J Pharm Sci 89:408–416.
24. Shamblin SL, Zografi G. 1998. Enthalpy relaxation in binary amorphous miztures containing sucrose. Pharm Res 15:1828–1834.
25. Andronis V, Zografi G. 2000. Crystal nucleation and growth of indomethacin polymorphs from the amorphous state. J Non-cryst Solids 271:236–248.

Sustained Release of Cisplatin from Multivesicular Liposomes: Potentiation of Antitumor Efficacy against S180 Murine Carcinoma

CHAOJU XIAO,[1] XIANRONG QI,[1] YOSHIE MAITANI,[2] TSUNEJI NAGAI[2]

[1]Department of Pharmaceutics, School of Pharmaceutical Sciences, Peking University, Beijing 100083, China

[2]Institute of Medicinal Chemistry, Hoshi University, Shinagawa-Ku, Tokyo 142-8501, Japan

Received 15 July 2003; revised 26 January 2004; accepted 7 February 2004

Published online 22 April 2004 in Wiley InterScience (www.interscience.wiley.com). DOI 10.1002/jps.20086

ABSTRACT: Cisplatin was encapsulated into multivesicular liposomes (MVLs) and the entrapment efficiency, size distribution, and *in vitro* drug release characteristics of the cisplatin-MVLs were studied. Pharmacokinetics, tissue distribution, and therapeutic efficacy of cisplatin-MVLs were compared against injection of cisplatin solution into mice inoculated with the murine carcinoma 180 (S180) tumor. The results showed that the cisplatin-MVLs were capable of high drug loading (0.148:1 mg cisplatin/mg lipid) and high encapsulation efficiency (>80%). The mean diameter of cisplatin-MVLs was 17 μm. *In vitro* studies of cisplatin-MVLs in saline solution showed that they sustained release of encapsulated drug for >7 days. Cisplatin-MVLs showed higher drug accumulation in the liver, spleen, and tumor regions than cisplatin solution, as well as higher plasma concentrations and a longer circulation time. The therapeutic efficacy of the cisplatin-MVL preparation against S180 tumor-bearing mice is significantly higher than that of cisplatin solution. © 2004 Wiley-Liss, Inc. and the American Pharmacists Association J Pharm Sci 93:1718–1724, 2004

Keywords: cisplatin; multivesicular liposomes; S180 tumor; sustained release; pharmacokinetics; therapeutic efficacy

INTRODUCTION

Cisplatin [*cis*-dichlorodiamine platinum (II)] is one of the most effective antitumor agents in the treatment of testicular, ovarian, head and neck, and lung cancer. However, its use is limited by significant undesirable side effects, such as nephrotoxicity, ototoxicity, neurotoxity, and myelosuppression to a lesser extent.[1] Several attempts to potentiate antitumor efficacy of cisplatin and reduce cisplatin-induced toxicities, including microspheres,[2] nanoparticles,[3] liposomes,[4] and polymer micelles[5] have been reported. Various types of liposomal formulations have been used as drug delivery vehicles to potentiate antitumor efficacy of cisplatin. However, in most cases, either unilamellar (ULVs) or multilamellar vesicles (MLVs) of cisplatin liposomes prepared by traditional methods offer low encapsulation efficacy and low drug loading.[6,7] The conventional methods of preparing liposomes, for example, reverse-phase evaporation vesicle (REV) method, are based on the passive entrapment of the drug during formation of the lipid bilayer vesicles, resulting in low encapsulation efficacy. Moreover, these processes require vigorous conditions, namely, organic solvents, sonication, and high temperature, which result in loss of drug efficiency and inactivation. Multivesicular liposomes (MVLs) prepared by a multiple emulsion method, are

Correspondence to: Xianrong Qi (Telephone: 86-10-82801584; Fax: 86-10-62015584; E-mail: qixr2001@yahoo.com.cn)

Journal of Pharmaceutical Sciences, Vol. 93, 1718–1724 (2004)

characterized by their unique structure of multiple, nonconcentric, aqueous chambers surrounded by a network of lipid membranes.[8] The structure of MVLs renders a higher aqueous volume-to-lipid ratio and much larger particle diameters compared with MLVs.[8,9] This technology facilitates loading of water-soluble drugs and improves their encapsulation efficacy. The active ingredient is encapsulated within the nonconcentric internal aqueous chambers and is released over an extended period of time. In a clinical trial in human patients with encapsulation of an antineoplastic agent, cytarabine, in MVLs maintained therapeutic cerebrospinal fluid concentrations over an extended period of time after a single intrathecal administration, which may improve therapeutic efficacy in patients with neoplastic meningitis.[10] MVLs containing cisplatin (cisplatin-MVLs) are also expected to have some degree of sustained release compared with ULVs or MLVs, and potentiate antitumor efficacy of cisplatin. Cisplatin, therefore, formulated in MVLs, was developed.

In the present study, cisplatin-MVLs were prepared. The release of cisplatin from the cisplatin-MVLs *in vitro* was studied. Pharmacokinetics, tissue distribution, and therapeutic efficacy of cisplatin-MVLs were compared with administration of cisplatin solution in mice inoculated with an S180 tumor using a single injection schedule in the tumor site. Cisplatin was entrapped into MVLs, with the aim of improving the entrapment efficiency, prolonging release time, improving drug localization in tumors, and enhancing antitumor efficacy.

MATERIALS AND METHODS

Materials and Animals

Cisplatin was purchased from Qilu Pharmaceutical Company (China). Egg phosphatidylcholine was purchased from Engel Bioengineer Company (China). Cholesterol was kindly provided by Wako Pure Chemical Industries, Ltd. (Japan). Triolein, free-base lysine, and other chemicals used were reagent grade. LACA mice were purchased from the Animal Institute of Health Science Center, Peking University.

Preparation of Cisplatin-MVLs and Cisplatin-REVs

Cisplatin-MVLs were prepared by a two-step, "water-in-oil-in-water," double emulsification process. The first step is the formation of a "water-in-oil" emulsion. A lipid combination of 4.5 μmol egg phosphatidylcholine, 4.5 μmol cholesterol, 2.0 μmol triolein, and 1.6 mg of co-membrane stabilizer was dissolved into 1.0 mL of chloroform-ether (1:1, v/v) and mixed with an equal volume of an aqueous solution containing cisplatin in 5.0% glucose (the first aqueous solution) in a 5-mL glass, screw-top vial. This mixture was sonicated to produce a water-in-oil emulsion (the first emulsion). A subsequent emulsification with 2.5 mL of a second aqueous solution in another glass vial, such as 4.5% glucose containing 40 mM lysine (the second aqueous solution), resulted in a water-in-oil-in-water double emulsion (the second emulsion). The vial was then vortexed for 10 s to decrease the size of chloroform-ether spherules. Chloroform-ether spherules suspended in the second aqueous solution were layered on the bottom of a 250-mL Erlenmeyer flask (bottom diameter, 8 cm). Chloroform and ether were removed by flushing nitrogen over the surface of the mixture at approximately 20°–37°C for 5 min. Decreasing turbidity of the suspension indicated near completion of solvent removal. The evaporation process was then allowed to proceed for a few more minutes until no odor of chloroform or ether was detectable.[8]

Cisplatin large ULV vesicles (cisplatin-REVs) were prepared by an REV method. Lipids used were the same as the cisplatin-MVLs formulation, and 3 mL of chloroform was added to the 50-mL round-bottom flask containing the lipid. The lipid solution was emulsified by sonicating for 5 min with 1 mL of aqueous solution, containing 1 mg of cisplatin in 5.0% glucose. The emulsion was transformed into a liposome suspension by removing organic solvents using a rotary evaporator at 30°C, under reduced pressure, for approximately 30 min. The size of cisplatin-REVs was in the range of 1–5 μm.

Determination of Encapsulation Efficacy

Cisplatin-MVL and cisplatin-REV preparations were centrifuged at 600*g* for 5 min to separate the free cisplatin (in the supernatant) from the liposomal cisplatin (in the pellet). The amount of cisplatin in the supernatant (C_f) and liposome pellet (C) was determined by flameless atomic absorbance spectroscopy (FAAS) (SPECTRAA 4.0; Varian, San Francisco, CA).[11] The amount of cisplatin in the initial preparation (C_t) was calculated from C and C_f. The weight of lipid in

the liposome pellet (L) was determined by enzymatic assay of phospholipids.[12] Because the total weight of lipids used in the formulation (L_t) was already known, entrapment efficiencies could be calculated using the following equation:

$$\text{Encapsulation efficacy (\%)} = (C/L)/(C_t/L_t) \times 100$$

In Vitro Release

Cisplatin-MVLs and cisplatin-REVs (1.39 mg lipid/mL) were centrifuged at 600*g* for 5 min and resuspended in saline solution. Aliquots of 100 μL were pipetted into 1.5-mL plastic-capped tubes containing 0.9 mL of saline solution. Each tube represented one time point, and the tubes were incubated at 37°C under dynamic conditions (rotation of 12 rpm). All *in vitro* release studies were set up three times at each time point, the tubes were centrifuged at 600*g* for 5 min, and the supernatants and pellets were separated. The samples of the supernatants were determined for cisplatin content by FAAS.

Animals and Tumor Models

Male LACA mice, each weighing about 22–30 g (4 weeks old), were used in pharmacokinetic, tissue distribution, and therapeutic efficacy studies. S180 cells were maintained by weekly transplantation of tumor cells into the peritoneal cavity. To obtain a suspension of tumor cells for transplantation, ascites fluid containing S180 cells was diluted to approximately 2×10^7 cells/mL with saline and 0.2 mL of the diluted suspension was injected subcutaneously per mouse.[13]

Pharmacokinetic and Tissue-Distribution Studies

Nine days after tumor inoculation, mice were injected at the tumor site[14] with either cisplatin solution or cisplatin-MVLs at a dose of 10 mg of cisplatin per kilogram of body weight. Each experimental time point consisted of three mice. Mice were sacrificed by cervical dislocation at indicated times after injection. Blood was collected by heart puncture and the heart, liver, spleen, lung, kidneys, and tumor were immediately removed. Tissues were carefully removed without any excess blood and weighed. Blood was collected in heparinized tubes and centrifuged to obtain the plasma fraction. Plasma and tissues were stored at −20°C until platinum analysis by FAAS.

Determination of Platinum in Plasma and Tissue Samples

Plasma and tissue samples, except the liver and tumor, were digested with HNO_3 (Newman et al., 1999), and the liver and tumor with HNO_3, H_2O_2, and a drop of *n*-octanol.[11] All samples were incubated at 85°C for 2 h, followed by centrifugation. Supernatant was diluted with double-distilled water to yield a final platinum concentration in the range of 50–400 ng/mL.

To determine the recovery of platinum, blank plasma and tissue samples were spiked with 2.0 mg of cisplatin, followed by digestion with HNO_3 or HNO_3 and H_2O_2 mixture, and then diluted with distilled water as described above. Platinum concentrations were determined by FAAS.

A calibration curve with platinum concentrations in the range of 50–400 ng/mL was run before analysis of each sample type. Values reported were the average of two separate platinum determinations for each sample. The recovery of platinum after incubation of plasma and tissues with cisplatin was 85–105%, and the RSD was 1.9–5.2%.

Therapeutic Efficacy Studies

Nine days after the mice were inoculated with the S180 tumor, they were treated by injection of cisplatin-MVLs or cisplatin solution into the tumor site at a dose of 10 mg of cisplatin per kilogram of body weight. The control group was injected with sterile saline solution instead. Each group consisted of eight mice. The tumor volume was measured daily with slide calipers every day after treatment. Each tumor volume was calculated by approximation of the solid tumor to an ellipsoid

$$V = k \times a \times b \times c$$

where V is the volume of the tumor (cm^3); a, b, and c are the length, width, and height (cm) of the tumor, respectively; and k is a constant.

Therapeutic efficacy was evaluated in terms of tumor growth rate and volume inhibited efficacy (VIE)[12]

$$\text{VIE} = (1 - V_T/V_C) \times 100\%$$

where V_T is the mean tumor volume of the cisplatin-MVLs or cisplatin solution group (treatment groups), and V_C is the mean tumor volume of the control group.

Statistical Analysis

Data from the animal experiments using mice were compared using analysis of variance and paired t test.

RESULTS AND DISCUSSION

Characterizations of Cisplatin-MVLs

Cisplatin was encapsulated at a high loading capacity of 0.148–0.444 mg of cisplatin per mg of lipid, and with good encapsulation efficacy into MVLs (>80%). Cisplatin was encapsulated into ULV liposomes, known as SPI-077, to reduce toxicity and prolong the circulating time in by intravenous injection.[6,15] The drug/lipid weight ratio of SPI-077 was 0.014:1 (mg/mg). It cannot be disregarded that the reticuloendothelial system function was saturated or damaged to some extent given that large quantities of lipid were administered.[16] Cisplatin-MVLs, with a drug/lipid weight ratio of 0.444:1, would contain a much lower amount of lipid than SPI-077, per given cisplatin dose.

Table 1 shows the stability of cisplatin-MVLs stored in 6° ± 2°C and 25° ± 2°C, respectively. The encapsulation efficacy of cisplatin at 6° ± 2°C did not decrease significantly after 3 months. There was no leakage of cisplatin from the MVLs over a 3-month period when stored at 6°C, indicating that the multivesicular matrix was stable in storage at 6°C over the indicated time period. The encapsulation efficacy of cisplatin at 25° ± 2°C was decreased from 95.7% to 83.0% after 3 months' storage, and there was a significant decrease of encapsulation efficacy at 40°C after 15 days (from 95.7% to 47.8%, data not shown), indicating that the leakage of cisplatin from the MVLs occurred when stored at 40°C.

A picture of cisplatin-MVLs under an optical microscope is shown in Figure 1. The cisplatin-MVLs were spherical. The median diameter of cisplatin-MVLs vesicle was 17 μm and 90% of vesicles were in the range of 5–25 μm.

MVLs are distinct from conventional liposomal (ULVs and MLVs) delivery systems in that each MVL encloses multiple nonconcentric internal chambers, and the average size of MVLs is about 10 times larger than the conventional liposomes.[8,17,18] Vesicle size can be modulated by the process parameters, especially by emulsification, to yield a water-in-oil-in-water emulsion. The size is not dependent on the first aqueous condition.

Figure 2 shows the *in vitro* release profiles for cisplatin-MVLs and cisplatin-REVs with the same formulation in saline at 37°C. At the time point of 168 h, there were many intact MVL spheres in solution under the light microscope. This result showed that the MVLs did not release completely in 168 h. In addition, there was some extent of absorbance between cisplatin and the lipids when the system reached equilibrium. The percentage of drug retained by the vesicles was plotted as a function of time release of the encapsulated cisplatin at the time points of 0, 0.17, 4, 8, 24, 72, and 168 h. The release profiles of cisplatin-MVLs and cisplatin-REVs were fitted with the Weibull Distribution. Using this equation, it was possible to calculate the time period required for the release of 50% of the solute load from the vesicular preparations ($t_{0.5}$).[19] The results showed that the $t_{0.5}$ for cisplatin-MVLs was 30.7 times greater than that of cisplatin-REVs.

MVL preparations can provide sustained release of entrapped drug without the "burst" effect or rapid initial release that is seen with the REVs. Because MVLs are different from ULV liposomes, such as REVs, a single breach in the external membrane of an MVL particle should not result in a total emptying of the solute load.

Pharmacokinetic and Tissue-Distribution Experiments

In the S180 tumor model mice, platinum concentrations were determined in the plasma and wet tissues of the heart, liver, spleen, lung, kidneys,

Table 1. Encapsulation Efficacy (%) of Cisplatin-MVLs Stored at Different Temperatures and Times *In Vitro*

	Time (Months)			
Temperature (°C)	0	1	2	3
6 ± 2	95.7 ± 1.2	96.3 ± 1.0	98.3 ± 1.4	98.6 ± 0.5
25 ± 2	95.7 ± 1.2	93.5 ± 0.4	92.1 ± 0.8	83.0 ± 0.5

Data are mean ± SD, $n = 3$.

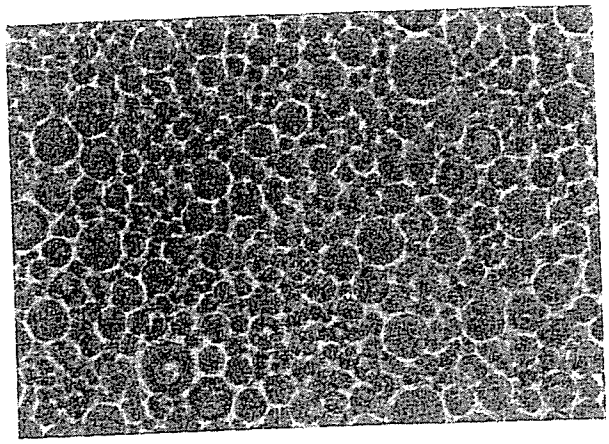

Figure 1. Optical micrograph of the cisplatin-MVLs suspended in saline solution at ×200 magnification, showing a spherical, honeycomb-like structure of tiny chambers and multivesicular nature.

and tumor at different time points after treatment. Pharmacokinetic and tissue-distribution analysis of drug disposition were based on the concentration of platinum in each tissue at the experimental time points 0.5, 8, and 48 h, respectively, after injection (as shown in Fig. 3).

The results indicated that Cisplatin-MVLs remained in the blood circulation for a significantly longer duration than an injection of cisplatin solution. After 8 h, the plasma concentration of cisplatin solution degraded to zero, but the concentration of cisplatin-MVLs was still high.

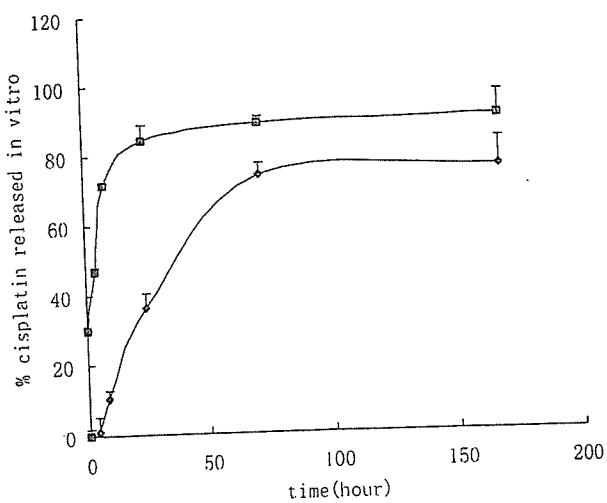

Figure 2. *In vitro* release characteristics of liposomes in saline solution under gentle rotating conditions (12 rpm) at 37°C. The data represent the mean ± SD, $n = 3$. ◆, cisplatin-MVLs; ■, cisplatin-REVs.

The most remarkable effect in this tissue-distribution study was the elevated concentration of platinum in the tumor site due to cisplatin-MVLs, as compared with cisplatin solution, reached to 2.5-, 4.0-, and 8.1-fold at 0.5, 8 and 48 h, respectively. This feature may be related to the capacity of cisplatin-MVLs to sustain release and accumulate at the tumor site. The figures indicated that cisplatin-MVLs in the organs relating to the mononuclear phagocytic system (liver and spleen) were higher than the cisplatin solution. These results suggest that a substantial amount of liposomes were transported and accumulated into the mononuclear phagocytic system. This effect may be related to the lipophilic properties of liposomes. The platinum concentration of cisplatin-MVLs in the heart was higher than that of cisplatin solution at each experimental point. This was because some liposomes were targeted to the cardiac muscle.[20] Cisplatin toxicity primarily affects renal function and the platinum of cisplatin-MVLs in this region was in the proximity of that for cisplatin solution at the three time points. This finding suggests that cisplatin-associated toxicity from cisplatin-MVLs might not be exacerbated. There were no significant differences between the groups treated with cisplatin-MVLs and cisplatin solution in the lung region. Whether cisplatin-MVLs are associated with increases in hepatic or splenic toxicity will require further investigation.

Therapeutic Efficacy

Four days after the mice were inoculated with the S180 tumor, the swells were found. Therapeutic efficacy was studied subsequent to a single injection on day 9 after S180 inoculation. Figure 4 charts the tumor growth rate in terms of mean tumor volume (cm^3) compared with the day before treatment for each day after treatment with cisplatin-MVLs or cisplatin solution. The result of paired t test for mean tumor volume, measured daily posttreatment for both preparations, showed significant difference between them ($p < 0.05$ after 9 days posttreatment. After 9 days post treatment, the mean tumor volume in the cisplatin-MVLs, cisplatin solution, and the control group were 2.12, 12.00, and 31.68 cm^3, respectively. According to the equation above, the VIE of the cisplatin-MVLs group (93.3%) and cisplatin solution group (62.1%) was calculated. The result showed that the VIE of the cisplatin-MVLs was 31.2% higher than that of the cisplatin solution group.

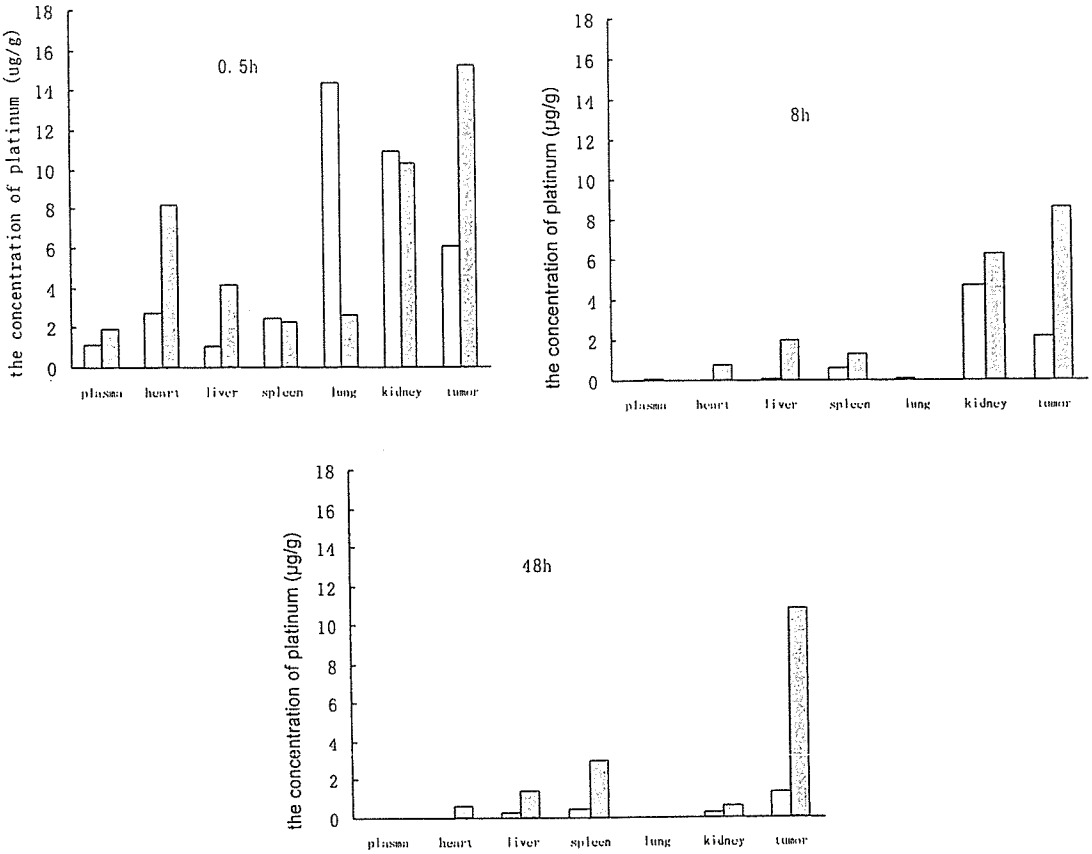

Figure 3. The platinum mean concentrations of different tissues at the experimental time points 0.5, 8, and 48 h, respectively. □, Cisplatim solution; □, cisplatin-MVLs; $n = 3$.

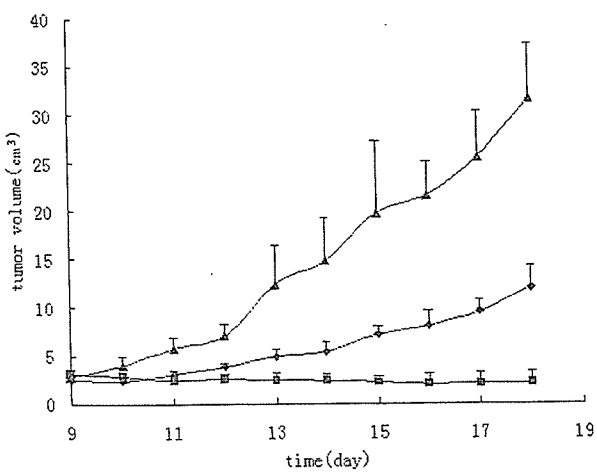

Figure 4. The tumor volume (cm^3) of mice inoculated with S180 tumor after treatment with the cisplatin solution (●), the cisplatin-MVLs (■), or the sterile saline for control (▲). Cisplatin solution or the cisplatin-MVLs was injected in the tumor site at a dose of 10 mg cisplatin/kg body weight. The data represent the mean ± SD, $n = 8$.

Studies of therapeutic efficacy indicate that cisplatin-MVLs had significant antitumor activity and were effective in reducing mean tumor volume of mice inoculated with S180 tumor, compared with the cisplatin solution group. When cisplatin-MVLs were injected in the tumor site, cisplatin solute was released from the MVL delivery system and exposed to tumor cells. Furthermore, as a result of the unique structure of cisplatin-MVLs, the rate of drug release was slow and the concentration of free cisplatin remained high at the tumor site—a combination that augmented tumoricidal efficiency.

CONCLUSIONS

The present findings indicate that the drug entrapment capability of cisplatin-MVLs is higher than cisplatin-REVs and their *in vitro* sustained-release profile of free cisplatin more suitable because of higher plasma concentrations and

prolonged circulation. The accumulation of drug in the liver, spleen, thymus, and tumor areas was higher for the cisplatin-MVLs preparation than that of cisplatin solution. The therapeutic efficacy of cisplatin-MVLs against S180 tumor-bearing mice is significantly higher than that of the cisplatin solution.

REFERENCES

1. Durant JR. 1980. Cisplatin: A clinical overview. In: Prestayko AW, Crooke ST, Carter SK, editors. Cisplatin: Current status and new developments. New York: Academic Press, pp 317–321.
2. Garcia-Contreras L, Abu-Izza K, Lu DR. 1997. Biodegradable cisplatin microspheres for brain implantation: Preparation and characterization. Pharm Dev Technol 2(1):53–65.
3. Avgoustakis K, Beletsi A, Panagi Z, Klepetsanis PG, Karydas AG, Ithakissios DS. 2002. PLGA-mPEG nanoparticles of cisplatin: *In vitro* nanoparticle degradation, *in vitro* drug release and *in vivo* drug residence in blood properties. J Control Release 79:123–135.
4. Steerenberg PA, Storm G, de Groot G, Claessen A, Bergers JJ, Franken MA, van Hoesel QG, Wubs KL, de Jong WH. 1988. Liposomes as a drug carrier system for *cis*-diamminedichloroplatinum(II). II. Antitumor resistance *in vivo*, induction of drug resistance, nephrotoxicity and Pt distribution. Cancer Chemother Pharmacol 21:299–307.
5. Mizumura Y, Matsumura Y, Hamaguchi T, Nishiyama N, Kataoka K, Kawaguchi T, Kawaguchi M, Hrushesky WJ, Moriyasu F, Kakizoe T. 2001. Cisplatin-incorporated polymeric micelles eliminate nephrotoxicity, while maintaining antitumor activity. Jpn J Cancer Res 92(3):328–336.
6. Newman MS, Colbern GT, Working PK, Engbers C, Amantea MA. 1999. Comparative pharmacokinetics, tissue distribution, and therapeutic effectiveness of cisplatin encapsulated in long-circulating, pegylated liposomes (SPI-077) in tumor-bearing mice. Cancer Chemother Pharmacol 43:1–7.
7. Freise J, Mueller WH, Magerstedt P, Schmoll HJ. 1982. Pharmacokinetics of liposome encapsulated cisplatin in rats. Arch Int Pharmacodyn Ther 258: 180–192.
8. Kim S, Turker MS, Chi EY, Sela S, Martin GM. 1983. Preparation of multivesicular liposomes. Biochim Biophys Acta 728:339–348.
9. Ye Q, Asherman J, Stevenson M, Brownson E, Katre NV. 2000. DepoFoam™ technology: A vehicle for controlled delivery of protein and peptide drugs. J Control Release 64:155–166.
10. Murry DJ, Blaney SM. 2000. Clinical pharmacology of encapsulated sustained-release cytarabine. Ann Pharmacother 34:1173–1178.
11. Li WJ. 1989. Determination of cisplatin in biological tissues and fluids by graphite furnace atomic absorption spectrometry. Chin J Pharm Anal 9: 82–85.
12. Qi XR, Maitani Y, Nagai T. 1995. Effect of soybean-derived sterols on the *in vitro* stability and the blood circulation of liposomes in mice. Int J Pharm 114:33–41.
13. Qi XR, Maitani Y, Nagai T, Wei SL. 1997. Comparative pharmacokinetics and antitumor efficacy of doxorubicin encapsulated in soybean-derived sterols and poly(ethylene glycol) liposomes in mice. Int J Pharm 146:31–39.
14. Anonymous. 2000. First phase II results of cisplatin/epinephrine in primary liver cancer. Oncology 14(1):89.
15. Colbern GT, Hiller AJ, Musterer RS, Working PK, Henderson IC. 1999. Antitumor activity of Herceptin® in combination with STEALTH® liposomal cisplatin or nonliposomal cisplatin in a HER2 positive human breast cancer model. J Inorg Biochem 77:117–120.
16. Bandak S, Goren D, Horowitz A, Tzemach D, Gabizon A. 1999. Pharmacological studies of cisplatin encapsulated in long-circulating liposomes in mouse tumor models. Anticancer Drugs 10:911–920.
17. Kim T, Murdane S, Gruber A, Kim S. 1996. Sustained-release morphine for epidural analgesia in rats. Anesthesiology 85(2):331–338.
18. Katre NV, Asherman J, Schaefer H, Hora M. 1998. Multivesicular liposome (DepoFoam™) technology for the sustained delivery of insulin-like growth factor-I (IGF-I). J Pharm Sci 87(11):1341–1346.
19. Xi NZ. 1996. Pharmaceutical science, 3rd ed. Beijing: People's Health Press, p 455.
20. Tang CS, Su JY, Li ZP, Zhang LZ, Yang J, Qi M, Liu FA, Tang J. 1992. The feasibility study of treating myocardial ischemia disease by the liposome-directed drug delivery system. Science in China (Series B) 2:165–171.

Novel Chitosan Particles and Chitosan-Coated Emulsions Inducing Immune Response via Intranasal Vaccine Delivery

Takahiro Nagamoto,[1] Yoshiyuki Hattori,[1] Kozo Takayama,[2] and Yoshie Maitani[1,3]

Received December 10, 2003; accepted January 5, 2004

Purpose. The aim of this study was to prepare a novel vaccine carrier particulate system (nanoparticles and emulsions) with chitosan and to evaluate the effect of this system on the immune response for intranasal delivery.

Methods. Chitosan nanoparticles (NP) and chitosan-coated emulsions (CC-Emul) were prepared by improvement of the method previously reported and by modified ethanol injection methods, respectively. The rats were immunized with the particles adsorbed with ovalbumin (OVA) and cholera toxin (CT) by intranasal (i.n.) and intraperitoneal (i.p.) administration.

Results. NP and CC-Emul could be prepared with particle diameter from about 0.4 μm to 3 μm. IgG induced by i.n. of NP was comparable with that by i.p., and IgA induced by i.n. of 0.4-μm- and 1-μm-size NP was significantly higher than control (OVA and CT). IgG and IgA induced by i.n. of 2-μm-size CC-Emul were significantly higher than those with control.

Conclusions. The novel chitosan particles used simple preparation methods showed high OVA adsorption. When administered intranasally, NP and CC-Emul induced systemic immune response in rats. These findings suggested that CC-Emul and the smaller-size (0.4 μm) NP are effective for targeting to nasal-associated lymphoid tissues (NALTs) in nasal vaccine delivery.

KEY WORDS: chitosan; emulsion; immune response; intranasal; nanoparticle.

INTRODUCTION

Mucosal vaccine delivery is very attractive for inducing a protective immune response because many pathogens invade the body through mucosal surfaces. The main function of mucosa-associated lymphoid tissue is the selective uptake of antigens and the induction of local immune responses (1). In nasal inoculation, particle antigens are mainly taken by the M-cell connected to the nasal-associated lymphoid tissues (NALTs), whereas soluble antigens are mainly absorbed at the nasal epithelium (2,3). Particle antigens will be processed at the NALT and preferentially drain to the antigen-presenting cells (APCs). Because emulsions are directed to lymph, the development of antigen particulate carrier systems (nanoparticle and emulsion) that allow mucosal vaccine delivery is of considerable interest.

Chitosan derived by the deacetylation of chitin, which is a polymer of D-glucosamine and *N*-acetyl-D-glucosamine, has high biodegradability and low toxicity. Chitosan particle delivery system can reduce the clearance rate from the nasal cavity, thereby increasing the contact time of the delivery system with the nasal mucosa (4). Chitosan suspensions or micro- and nanoparticles have been reported to have immune stimulating activity such as increasing accumulation and activation of macrophage and polymorphonuclear cell, promoting resistance to infections by microorganisms, and inducing cytokines (5). Among the various particle properties, the effective particle size on immune responses appears to be a key factor but has not been intensively investigated. The uptake of chitosan micro- (>1 μm) and nanoparticles from the nasal cavity was reported in the past decade (5,6). However, the optimal size of particles remains unclear for intranasal vaccine delivery. Although numerous nanoparticle preparation methods are known, sufficient antigen loading of nanoparticles and emulsions remains a challenge. Therefore, various-size novel chitosan particles and chitosan-coated emulsions loaded with antigen were prepared.

The aim of this study was to prepare and characterize chitosan nanoparticles and chitosan-coated emulsions for adsorptive loading of ovalbumin (OVA) and to evaluate the effect of particle size of chitosan nanoparticles (NP) and chitosan-coated emulsion (CC-Emul) loaded with OVA and cholera toxin (CT) on the immune response for intranasal vaccine delivery.

MATERIALS AND METHODS

Chemicals

Soybean oil and three kinds of chitosan (chitosan 10, chitosan 100, and chitosan 500 with a deacetylation degree of about 80 mol% with molecular weights of 10 kDa, 100 kDa, and 500 kDa, respectively) were purchased from Wako Pure Chemical Industries, Ltd. (Osaka, Japan). OVA was obtained from Worthington Biochemical Corporation (Lakewood, NJ, USA), and CT obtained from Biomol Research Laboratories, Inc. (Plymouth Meeting, PA, USA). Eight-week-old male Wistar Kyoto Rats (WKY rat) were purchased from Oriental Yeast, Co. Ltd. (Tokyo, Japan). Tween 80 and oleic acid (OA) were purchased from Tokyo Kasei Kogyo Co. Ltd. (Tokyo, Japan). Egg phosphatidylcholine (EPC) was from QP Co. Ltd. (Tokyo, Japan). All other reagents were of analytical grade.

Preparation of NP

Three different size NP (average diameters of about 700 nm, 1300 nm, and 3000 nm for individual batches) were prepared using chitosan 10, chitosan 100, and chitosan 500, respectively, by improvement of methods previously reported by Lubben *et al.* (7). Briefly, 0.25% (v/v) of chitosan 10, chitosan 100, and chitosan 500 solutions were prepared in 2% acetic acid aqueous solution. Then, 1 ml of 10% (w/v) sodium sulfate was added to 100 ml of each chitosan solution. Moreover, to obtain smaller NP, the NP sample prepared by chi-

[1] Institute of Medicinal Chemistry, Hoshi University, Ebara 2-4-41, Shinagawa, Tokyo 142-8501, Japan.
[2] Department of Pharmaceutics, Hoshi University, Ebara 2-4-41, Shinagawa, Tokyo 142-8501, Japan.
[3] To whom correspondence should be addressed. (e-mail: yoshie@hoshi.ac.jp)

ABBREVIATIONS: APC, antigen presenting cell; CC-Emul, chitosan-coated emulsions; CT, cholera toxin; EPC, egg phosphatidylcholin; NALTs, nasal-associated lymphoid tissues; NP, chitosan nanoparticles; OA, oleic acid; OVA, ovalbumin.

0724-8741/04/0400-0671/0 © 2004 Plenum Publishing Corporation

tosan 10 in a diameter of 700 nm was sonicated to reduce the particle size to 300 nm. After preparation of NP with different sizes, samples were centrifuged for 1 h at 48,000 rpm for 300-nm NP and at 10,000 rpm for other-sized NP, respectively. After the pellets were freeze-dried overnight, the 40-mg resultant pellets were resuspended in 1 ml of 0.2% (w/v) Tween 80 solution at pH 11.0 to adjust nanoparticle suspension at pH 6.0. For the administration dosage form, 0.01 mg CT and 20 mg OVA were added to 1 ml of resultant NP and incubated at room temperature overnight.

Preparation of CC-Emul

Emulsions with the size of 0.4 μm and 0.7 μm were prepared by a modified ethanol injection method (8). Briefly, 100 mg of soybean oil, 60 mg of EPC, and 60 mg of OA were dissolved in 5 ml hot ethanol, and then 10 ml Milli Q water was added. After ethanol was removed with part of Milli Q water, 5-ml emulsions formed. Then, 0.25 ml of the aqueous solution dissolved with 2 mg Tween 80 and 2 mg chitosan 10 was added to 0.25 ml of the 0.4-μm-size emulsion (total oil and lipid 44 mg/ml) adjusted to about pH 5.0 by 0.1 M NaOH. Chitosan-coated emulsion (CC-Emul, sized 0.4 μm) was prepared by addition of 20 mg of OVA and 0.01 mg of CT to a final volume of 1 ml of the above emulsions with shaking at room temperature overnight. CC-Emul sized 2 μm was prepared as above except using 0.7-μm-size emulsion and double the amounts of each component and addition of Milli Q water slowly by the modified ethanol injection method. This emulsion was diluted 2-fold before use for CC-Emul sized 2 μm.

The cumulant diameter and ζ-potential of the particles in water were measured by the dynamic and electrophoretic light-scattering method, respectively, using a laser light-scattering instrument (Model ELS-800, Otsuka Electronics, Osaka, Japan).

Determination of OVA Adsorption Amount to NP and CC-Emul

The relative adsorption amount of OVA to NP and CC-Emul was calculated by determining the amount of protein remaining in the supernatant after centrifugation at 48,000 rpm, using bicinchonic acid (BCA) protein assay kit (Pierce, Rockford, IL, USA). The adsorption ratio was estimated using the following equation;

$$\text{Adsorption ratio (\%)} = \frac{\text{OVA}_{\text{total conc.}} - \text{OVA}_{\text{superntant conc.}}}{\text{OVA}_{\text{total conc.}}} \times 100$$

Immunization Protocol and Enzyme-Linked Immunosorbent Assay

Each group of rats was immunized by i.n. and i.p. with one of the following vaccine formulations on days 0, 14, and 28, following the method of Staats *et al.* (9). Fifty microliters of the various-size NP and CC-Emul were administered as approximately 200 g to rats via one nostril with a polyethylene tube. Control rats received the same concentration of OVA and CT in 0.2% (w/v) Tween 80 Milli Q solution.

Blood samples were collected from the jugular vein–anesthetized rats (receiving pentobarbital at a dose of 50 mg/kg following i.p.) via i.p. and i.n. administration on day 35. Sera were separated by centrifugation at 13,000 rpm for 4 min and were stored at 4°C.

Concentrations of IgG and IgA in serum were measured according to the Rat IgG and IgA ELISA Quantitation Kit (Bethyl Laboratories, Montgomery, TX, USA). Titration of rat anti-OVA IgG in serum was measured according to the anti-ovalbumin IgG ELISA Kit (Genesis Diagnostics Ltd, Cambridgeshire, UK).

Statistical Analysis

All values are expressed as means ± SD. Statistical significance of the data was evaluated by Student's *t* test. A p value of 0.05 or less was considered significant. All experiments were repeated at least three times.

RESULTS AND DISCUSSION

Characterization of NP

Considering the toxicity of Tween 80, we prepared NPs by decreasing the concentration of Tween 80. This method showed the size of NP smaller than the method by Lubben *et al.* (7). The characterization of NP is summarized in Table I. The particle size of NP was increased with increasing molecular weights of chitosan. OVA adsorption into NP decreased the ζ-potentials, but remained positive in ζ-potential (about 25 mV) although the adsorbed ratio of OVA was relatively high at greater than 80%. The release of OVA from NP was not observed during 3 h in PBS solution pH 7.2 at 37°C (data not shown).

Particulate vaccine delivery carrier should be targeted to lymphoid tissue as antigen sampling cells provide access to mucosal lymphoid tissue (7). Because the M-cells connecting lymphoid tissue take up antigens and microparticles smaller than 10 μm, particulate systems for antigen drug delivery require micro-size particles to be taken up by M-cells, neither by epithelial cells, nor by drug release upon arrival at the mucosae. Therefore, it was expected that as the particle size of NP obtained in this study was relatively small and the amount of OVA released from NP was low, vaccination may be effectively achieved.

Characterization of CC-Emul

With the addition of chitosan solution at weight ratios greater than 0.1 of chitosan to total oil and lipids in the emulsions, the average diameters of particles became almost con-

Table I. Characterization of NP Without Cholera Toxin

NP (μm)	OVA*	Average diameter (nm)	ζ-potential (mV)	Adsorbed OVA† (%)
0.4	–	310 ± 3.6	27.3 ± 0.5	
	+	385 ± 8.5	24.7 ± 0.6	84.8 ± 0.3
1	–	692 ± 13.6	28.7 ± 0.9	
	+	1102 ± 80	24.7 ± 0.3	89.1 ± 2.0
2	–	1355 ± 168.2	29.3 ± 3.4	
	+	2048 ± 313	25.4 ± 0.6	88.0 ± 1.1
3	–	3080 ± 147.7	32.2 ± 3.9	
	+	3287 ± 419	25.6 ± 0.4	78.9 ± 0.4

NP, chitosan nanoparticles; OVA, ovalbumin. Data are Mean ± SD (n = 3).

* Chitosan nanoparticles (40 mg) adsorbed OVA (20 mg). NP (0.4 and 1 μm), NP (2 μm), and NP (3 μm) were prepared using chitosan 10, 100, and 500, respectively.

† Calculated from the amount of free OVA determined using the BCA protein assay kit.

Table II. Characterization of Chitosan-Coated Emulsion with Ovalbumin (OVA) and Cholera Toxin (CT)*

Emulsions	Average diameter (nm)	ζ-potential (mV)	Adsorbed OVA† (%)
Emulsion (0.4 μm)	362.1 ± 8.4	−48.8 ± 4.1	
Chitosan-coated‡	362.2 ± 13.0	17.0 ± 0.6	
+ OVA and CT§	391.0 ± 6.6	10.2 ± 1.6	96.6 ± 0.2†
Emulsion (2 μm)	729.6 ± 26.6	−48.6 ± 0.9	
Chitosan-coated	897.3 ± 274.1	14.3 ± 2.3	
+ OVA and CT§	1811.3 ± 15.0	10.3 ± 0.8	105.0 ± 11.4†

Data are mean ± SD (n = 3).
* Chitosan-coated emulsion adsorbed OVA and CT (CC-Emul).
† Calculated from the amount of free OVA determined by BCA protein assay kit.
‡ Chitosan 2 mg, total oil and lipid of emulsion 11 mg per ml.
§ OVA 20 mg, CT 0.01 mg per ml of chitosan-coated emulsion.

stant. Corresponding to the change of size, the ζ-potential of negatively charged emulsions became positive by coating chitosan (data not shown). Therefore, for further experiments, the 0.15 weight ratio of chitosan was used to the total oil and lipids of the emulsion for CC-Emul as the chitosan adsorption may be saturated.

After the addition of chitosan to the emulsion, the average diameters of the emulsions increased slightly, while the ζ-potential of the emulsions sized 0.4 μm and 0.7 μm with about −49 mV became 17 mV and 14.3 mV, respectively (Table II). Furthermore, after the addition of OVA and CT, the 362-nm and 897-nm approximate diameters of CC-Emul were increased to 391 nm and 1811 nm, respectively, and their ζ-potential decreased to about 10 mV. The adsorbed ratio of OVA to CC-Emul was nearly 100% (Table II). These results suggested that adequate amounts of chitosan to bind OVA completely existed on the surface of the emulsions. These CC-Emul represent CC-Emul sized 0.4 μm and 2 μm, respectively, from the final size of emulsions. The OVA released from CC-Emul was not detected after 3 h incubation in PBS solution pH 7.2 at 37°C (data not shown). Relatively smaller CC-Emul particles appeared to be more stable than larger ones.

Immunization Following i.p. and i.n. Administration of NP

Figure 1 shows the immune activity of antibody at 35 days after the first immunization following i.p. and i.n. administration of NP. NP following i.p. administration induced significantly higher IgG than control (Fig. 1A). Chitosan has a positive charge and adjuvant activity after i.p. administration in mice (10). Our finding may correspond to the report; the positively charged liposomes are effectively transferred to APC rather than negatively charged ones by i.p. administration (11).

NP following i.n. administration induced significantly higher IgG antibody response compared with control (Figs. 1A and 1B). Production of anti-OVA IgG obtained in this immunization study was comparable to that of IgG in the blood (data not shown). NP sized 0.4 μm and 1 μm showed significantly higher production of IgA compared with the 3-μm-size NP. The uptake of chitosan microparticles has previously been reported (6), but not that of nanoparticles. The reason might be due to the recongnition of NPs by M cells.

Microparticles are retained in the M-cells and induce mucosal immunity, whereas nanoparticles can also be taken up from the NALTs and also induce systemic immunity. Uchida *et al.* reported that 4-μm-size synthetic polymer particles showed higher IgG antibody response than 1.3-μm-size ones for oral administration (12). Jung *et al.* (13) reported that the oral and i.n. administration of the about 0.5-μm-size synthetic polymer particles with negative ζ-potential increased IgG, but those of particles >1 μm did not. However, in the current results, there was no significant difference in the IgG production between the different-size NP following i.n. administration.

Immunization Following i.p. and i.n. Administration of CC-Emul

Although i.p. application of CC-Emul did not increase IgG production compared with control (Fig. 2A), IgA levels

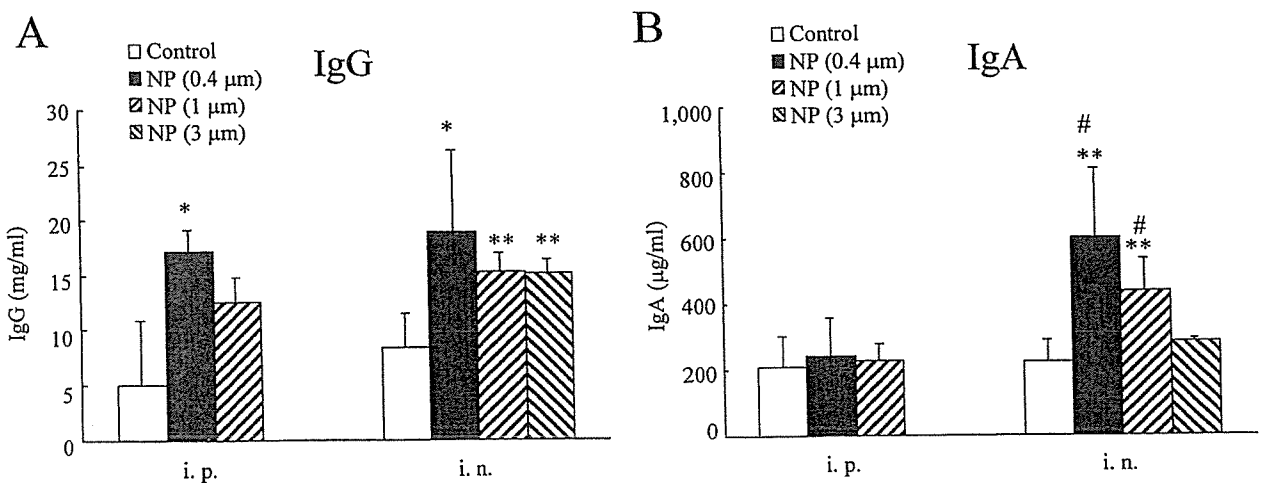

Fig. 1. The (A) IgG and (B) IgA concentrations from rats (n = 3 to 5) immunized by i.p. and i.n. on days 0, 14, and 28 with OVA (5 mg/kg) and CT (2.5 μg/kg) alone for control and NP in Milli Q water. The particle diameter of NP is approximately 0.4 μm, 1 μm, and 3 μm. The sera were collected on day 35. Data are mean ± SD. *$p < 0.05$ and **$p < 0.01$ compared with control, and #$p < 0.05$ compared with NP (3 μm).

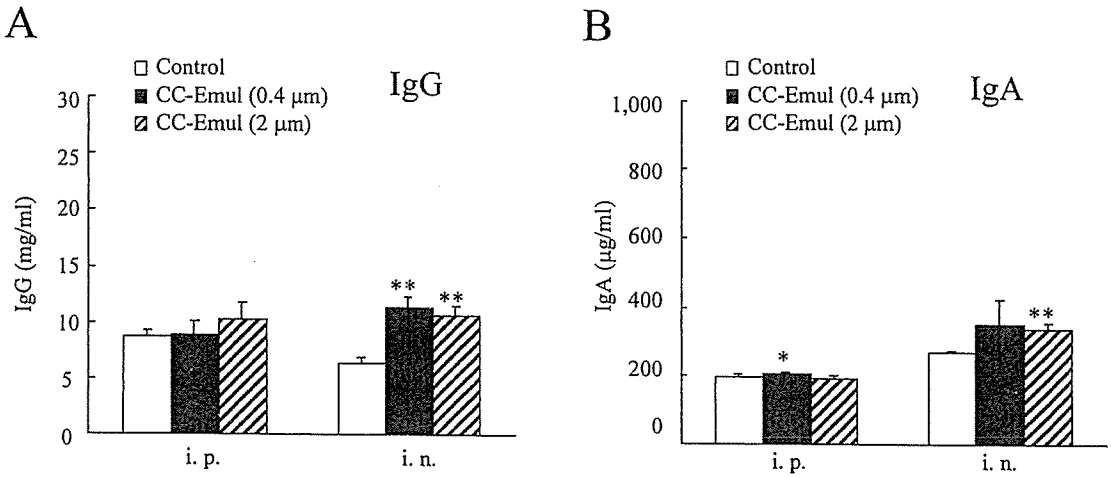

Fig. 2. The (A) IgG and (B) IgA concentrations from rats (n = 3 to 5) immunized by i.p. and i.n. on days 0, 14, and 28 with OVA (5 mg/kg) and CT (2.5 μg/kg) alone for control and CC-Emul in Milli Q water. The particle diameter of CC-Emul is approximately 0.4 μm and 2 μm. The sera were collected on day 35. Data are mean ± SD *$p < 0.05$ and **$p < 0.01$ compared with control.

were similar to those by NP (Fig. 2B). Intranasal administration of CC-Emul sized 2 μm showed significantly higher IgG and IgA antibody responses compared with control. Antibody responses after i.n. administraion between NP and CC-Emul were not different, and each antibody reached similar levels in both particles. No significant difference of IgG and IgA productions was seen between 0.4-μm- and 2-μm-size CC-Emul. This finding corresponds well to NP.

CC-Emul after i.p. administration did not increase IgG production. The reason was not clear, but basically emulsions are easily transferred to lymphoid tissue, so this might render the effect of particle size for immunization by CC-Emul irrelevant. Nevertheless, further experiments are needed to elucidate the difference in the production of antibody by formulations.

CONCLUSIONS

The novel chitosan particles (nanoparticles and emulsions) used simple preparation methods showed high OVA adsorption. OVA was hardly released from each formulation, suggesting that the developed particulate vaccine system may retain antigen on particles until uptake into mucosal membrane. Moreover, chitosan nanoparticles and emulsions administered i.n. induced a significantly higher immune response compared with control, and also, this response was comparable with i.p. injection. From these findings, the chitosan particulate system for nasal vaccine delivery could be a promising candidate.

ACKNOWLEDGMENTS

This project was supported in part by a grant from The Promotion and Mutual Aid Corporation for Private Schools of Japan and by a Grant-in-Aid for Scientific Research from the Ministry of Education, Culture, Sports, Science, and Technology of Japan. We are grateful to Dr. K. Nakamura for his fruitful discussion and to Mr. K. Noguchi and Ms. M. Itabashi for their technical assistance.

REFERENCES

1. M. R. Neutra, E. Pringault, and J. P. Kraehenbuhl. Antigen sampling across epithelial barriers and induction of mucosal immune responses. *Annu. Rev. Immunol.* **14**:275–300 (1996).
2. A. J. Almeida and H. O. Alpar. Nasal delivery of vaccines. *J. Drug Target.* **3**:455–467 (1996).
3. A. de Haan, H. J. Geerligs, J. P. Huchshorn, G. J. van Scharrenburg, and A. M. Palache, and J. Wilschut. Mucosal immuneadjuvant activity of liposomes: induction of systemic IgG and secretory IgA antibody responses in mice by intranasal immunization with an influenza subunit vaccine and coadministered liposomes. *Vaccine* **13**:155–162 (1995).
4. R. J. Soane, M. Frier, A. C. Perkins, N. S. Jones, S. S. Davis, and L. Illum. Evaluation of the clearance characteristics of bioadhesive systems in humans. *Int. J. Pharm.* **178**:55–65 (1999).
5. I. M. van der Lubben, J. C. Verhoef, G. Borchard, and H. E. Junginger. Chitosan for mucosal vaccination. *Adv. Drug Deliv. Rev.* **52**:139–144 (2001).
6. I. M. van der Lubben, J. C. Verhoef, G. Borchard, and H. E. Junginger. Chitosan and its derivatives in mucosal drug and vaccine delivery. *Eur. J. Pharm. Sci.* **14**:201–207 (2001).
7. I. M. Van Der Lubben, F. A. Konings, G. Borchard, J. C. Verhoef, and H. E. Junginger. In vivo uptake of chitosan microparticles by murine Peyer's patches: visualization studies using confocal laser scanning microscopy and immunohistochemistry. *J. Drug Target.* **9**:39–47 (2001).
8. Y. Maitani, H. Soeda, J. Wang, and K. Takayama. Modified ethanol injection method for liposome containing β-sitosterol β-D-glucoside. *J. Liposome Res.* **11**:115–125 (2001).
9. H. F. Staats and F. A. Ennis. IL-1 is an effective adjuvant for mucosal and systemic immune responses when coadministered with protein immunogens. *J. Immunol.* **162**:6141–6147 (1999).
10. K. Nishimura, S. Nishimura, N. Nishi, F. Numata, Y. Tone, S. Tokura, and I. Azuma. Adjuvant activity of chitin derivatives in mice and guinea-pigs. *Vaccine* **3**:379–384 (1985).
11. T. Nakanishi, J. Kunisawa, A. Hayashi, Y. Tutumi, T. Hayakawa, and T. Mayumi. Enhancement of liposome adjuvant actions for tumor vaccines by increasing the degree of positive surface charge. *Drug Delivery System* **13**:151–157 (1998).
12. T. Uchida and S. Goto. Oral delivery of poly(lactide-co-glycolide) microspheres containing ovalbumin as vaccine formulation: particle size study. *Biol. Pharm. Bull.* **17**:1272–1276 (1994).
13. T. Jung, W. Kamm, A. Breitenbach, K. D. Hungerer, E. Hundt, and T. Kissel. Tetanus toxoid loaded nanoparticles from sulfobutylated poly(vinylalcohol)-graft-poly(lactide-co-glycolide): evaluation of antibody response after oral and nasal application in mice. *Pharm. Res.* **18**:352–360 (2001).

Available online at www.sciencedirect.com
SCIENCE DIRECT®
Journal of Controlled Release 97 (2004) 173–183
journal of controlled release
www.elsevier.com/locate/jconrel

Enhanced in vitro DNA transfection efficiency by novel folate-linked nanoparticles in human prostate cancer and oral cancer

Yoshiyuki Hattori*, Yoshie Maitani

Institute of Medicinal Chemistry, Hoshi University, Ebara 2-4-41, Shinagawa, Tokyo, 142-8501, Japan

Received 2 September 2003; accepted 6 March 2004

Available online 17 April 2004

Abstract

Novel folate-linked, cationic nanoparticles (NPs) were developed and evaluated for potential use for gene delivery to human oral cancer (KB cells) and human prostate cancer (LNCaP cells), which abundantly expressed folate binding proteins. Folate-polyethylenglycol-distearoylphosphatidylethanolamine conjugate (f-PEG-DSPE) was incorporated in NPs composed of 3([*N*-(*N'*,*N'*-dimethylaminoethane)-carbamoyl] cholesterol (DC-Chol) and Tween 80. NP-0.3FT, -1FT and -1FLT, which contain 0.3 and 1 mol% f-PEG_{2000}-DSPE, and 1 mol% f-PEG_{5000}-DSPE, respectively, showed about 100–200 nm in size. The NP/plasmid DNA complex (nanoplex) remained in an injectable size (230–340 nm) and slightly increased its size in serum. The association of NP-1FT with KB cells was enhanced by f-PEG_{2000}-DSPE and was blocked by co-incubation with free folic acid in medium. In transfection activity, the NP-1FT, but not NP-1FLT, showed high activity into KB and LNCaP cells in the presence of serum. The NP-0.3FT also showed high activity into LNCaP cells, but not KB cells. In RT-PCR analysis, KB cells strongly expressed folate receptors mRNA, but LNCaP cells did not. In contrast, LNCaP cells expressed mRNA of prostate-specific membrane antigen (PSMA), which interacts with the folate substrate. Uptake mechanism of folate-linked NPs in LNCaP cells may be different from that in KB cells. This is the first report that folate-linked NPs selectively deliver the DNA to LNCaP cells, suggesting that such NPs are potentially targeted vectors to prostate cancer for gene delivery.

Keywords: Cationic nanoparticles; Folic acid; Gene delivery; KB; LNCaP

1. Introduction

Gene therapy has become an increasingly important strategy for treating a variety of human disease, including cancer [1]. The development of suitable delivery vectors for in vivo gene transfer is necessary for the clinical application of therapeutic genes. Synthetic vectors such as a lipid nanoparticle (liposome and emulsion) have become an attractive strategy due to their lack of immunogenicity, the potential for tissue-specific targeting, relative safety and relative ease of large-scale production. The use of cationic liposome/DNA complex (lipoplex) has become one of the most promising methods for in vivo gene delivery [2]. However, cationic liposomes mixed with DNA

* Corresponding author. Tel./fax: +81-3-5498-5048.
E-mail address: yhattori@hoshi.ac.jp (Y. Hattori).

0168-3659/$ - see front matter © 2004 Elsevier B.V. All rights reserved.
doi:10.1016/j.jconrel.2004.03.007

often result in large aggregated lipoplexes [3,4], which cannot be injected in blood vessels and yield very low-level transfection efficiency in vivo [5,6]. Such vectors could be used to achieve an injectable particle size after forming complex with DNA, with resulting high transfection efficiency.

Tissue-targeted gene expression is also an important issue for improvement of safety in gene therapy. A variety of targeting ligands has been examined for targeting liposomes including folate receptors [7–12]. Folate receptor (FR) is known to be abundantly expressed in large fraction of human tumors, but it is only minimally distributed in normal tissues [13–19]. Therefore, the FR serves as an excellent tumor marker as well as a functional tumor-specific receptor.

Folic acid, a high-affinity ligand for FR, retains its receptor-binding and endocytosis properties when covalently linked to a wide variety of molecules. Therefore, the liposomes conjugated to folate ligand via PEG-spacer have been used for the delivery of chemotherapeutic agent to the receptor-bearing tumor cells, e.g. human oral cancer (KB) cells [12]. However, the use of folate ligand as a targeting ligand to deliver DNA has not been successful in in vivo gene therapy [9,10].

Prostate cancer is a significant problem, reported as the leading cancer diagnosed in males [20]. High affinity folate binding protein was characterized in human prostate [21], but the kind of folate binding protein expressed in human prostate has not been reported.

Prostate-specific membrane antigen (PSMA) is a transmembrane protein with an overexpressed pattern specific to human prostate cancer cell line (LNCaP cells) and malignant human prostate tissue [22]. The physiological role of PSMA in prostate cancer remains unknown. It shows hydrolase enzymic activity with a folate substrate [23]. If overexpression of PSMA in prostate cancers represents an advantageous adaptation that allows uptake of folic acid required for rapid division, it could be utilized as a potential target for selective delivery.

In the present study, we prepared folate-linked nanoparticles (NPs) consisting of 3([*N*-(*N'*,*N'*-dimethylaminoethane)-carbamoyl] cholesterol (DC-Chol), Tween 80 and folate-polyethylenglycol-distearoylphosphatidylethanolamine conjugate (f-PEG-DSPE) to form injectable particle-sized complex with DNA (nanoplex) and to maintain the particle size of nanoplexes in serum. Furthermore, we examined the ability of folate linked at the distal end of PEG_{2000}-DSPE to enhance the gene expression in KB and LNCaP cells, and then investigated the uptake mechanism by examining the expression pattern of FRs and PSMA mRNAs in both cells by the RT-PCR method.

2. Materials and methods

2.1. Materials

DC-Chol was purchased from Sigma (St. Louis, MO, USA). Tween 80 (mean M.W.: 1300 Da) and Triton X-100 were obtained from Tokyo Kasei Kogyo (Tokyo, Japan). Folic acid and ninhydrin spray were purchased from Wako (Tokyo, Japan). PEG-lipid (polyethyleneglycol derivative of distearoylphosphatidylethanolamine, PEG-DSPE, mean molecular weight of PEG: 2000 and 5000 Da) was supplied by NOF (Tokyo, Japan). Tfx20, cationic liposome component mixed with L-dioleoylphosphatidylethanolamine (DOPE), was purchased from Promega (Madison, WI, USA). 1,1'-Dioctadecyl-3,3,3',3'-tetramethylindocarbocyanine perchlorate (DiI) was obtained from Lambda Probes and Diagnostics (Graz, Austria). Silica gel 60 F_{254} was purchased from Merck (West Point, PA, USA). The Pica gene luciferase assay kit was purchased from Toyo Ink (Tokyo, Japan). Bicinchonic acid (BCA) protein assay reagent was purchased from Pierce (Rockford, IL, USA). All other chemicals used were of reagent grade. The plasmid DNA (about 6740 bp) encoding the luciferase maker gene under the CMV promoter (pCMV-Luc) was supplied by Dr. Tanaka in Mt. Sinai School of Medicine (NY, USA). All reagents were of analytical grade. Folate-deficient RPMI1640 medium and fetal bovine serum were purchased from Life Technologies (Grand Island, NY, USA).

2.2. Synthesis of f-PEG_{2000}-DSPE and f-PEG_{5000}-DSPE

f-PEG_{2000}-DSPE was synthesized as reported previously [24]. Folic acid was dissolved in dimethyl sulfoxide (1 ml). Amino-PEG_{2000}-DSPE (100 mg,

0.035 mmol) and pyridine (0.5 ml) were added to the folic acid solution followed by dicyclohexylcarbodiimide (32.5 mg). The reaction was continued at room temperature for 4 h. TLC on silica gel 60 F_{254} (75:36:6 chloroform/methanol/water) showed a new spot (R_f=0.57) due to the formation of the product. The disappearance of amino-PEG_{2000}-DSPE (R_f=0.76) from the reaction mixture was confirmed by ninhydrin spray. Pyridine was removed by rotary evaporation. Water (12.5 ml) was added to the reaction mixture. The solution was centrifuged to remove trace insolubles. The supernatant was dialyzed in Spectra/Por CE (Spectrum, Houston, TX, USA) tubing (MW cutoff of 300,000 Da) against saline (50 mM, two times with 2000 ml) and water (three times with 2000 ml). The dialyzed product was lyophilized and analyzed by ESI-TOFMS mass spectroscopy. Exactly the same protocol was used to prepare f-PEG_{5000}-DSPE from amino-PEG_{5000}-DSPE.

2.3. Plasmid DNA

Protein-free preparation of pAAV-CMV-Luc plasmid was purified following alkaline lysis using maxiprep columns (Qiagen, Hilden, Germany). FITC-labeled plasmid was prepared with Label IT fluorescein labeling kit (Mirus, Madison, WI, USA).

2.4. Preparation of NPs

NP formulae in Table 1 were prepared with lipids (DC-Chol, Tween 80, PEG_{2000}-DSPE, f-PEG_{2000}-DSPE and/or f-PEG_{5000}-DSPE) in 10-ml water by the modified ethanol injection method. In DiI-labeled NPs, DiI was incorporated at 0.04 mol% of the total lipid. Briefly, an appropriate volume of ethanol containing lipids was prepared. The ethanol was removed using an evaporator and finally a semisolid solution was formed. An appropriate volume of water was added to the semisolid solution, and the ethanol contained in the solution was removed by an evaporator. To obtain a uniform particle size distribution, the mixture was sonicated for 5 min in a bath-type sonicator (Honda Electronics, W220R, 200 W, 40 kHz, Tokyo, Japan) and then sterilized by filtration through a sterile syringe-driven filter unit with a pore size of 450 nm at once.

Table 1
Formulae of FR-targeted nanoparticles

Formulation	Mol%				
	DC-Chol	Tween 80 (T)	PEG_{2000}-DSPE (P)	f-PEG_{2000}-DSPE (F)	f-PEG_{5000}-DSPE (FL)
NP-T	95	5	–	–	–
NP-0.3PT	94.7	5	0.3	–	–
NP-1PT	94	5	1	–	–
NP-0.3FT	94.7	5	–	0.3	–
NP-1FT	94	5	–	1	–
NP-1FLT	94	5	–	–	1

Nanoparticles were prepared with lipids [e.g. DC-Chol/Tween 80/f-PEG_{2000}-DSPE=94/5/1, molar ratio=10:1.3:0.65, weight (mg)] in 10-ml water by the modified ethanol injection method.

2.5. Size and ζ-potential of NPs and nanoplexes

The particle size distributions of NPs and nanoplexes were measured by the dynamic light-scattering method, and the ζ-potentials of NPs and nanoplexes were determined by the electrophoresis light-scattering method (ELS-800, Otsuka Electronics, Osaka, Japan) at 25 °C after by diluting of dispersion to an appropriate volume with water. Stability of NPs was assessed by measuring size changes after 60 days. The nanoplex containing plasmid DNA and NPs at the charge ratio (+/−) of 1/1, 3/1 or 5/1 was used to measure the size and ζ-potential. Stability of nanoplex was assessed by measuring size changes after dilutions in 10% or 50% serum.

2.6. Cell culture

KB cells were supplied from Cell Resource Center for Biomedical Research, Tohoku University. LNCaP cells were from the Department of Urology, Keio University Hospital. KB and LNCaP cells were grown in folate-deficient RPMI-1640 medium supplemented with 10% heat-inactivated serum and kanamycin (100 μg/ml) at 37 °C in a 5% CO_2 humidified atmosphere.

2.7. Association of nanoplexes with KB cells

KB cell cultures were prepared by plating KB cells in a 35-mm culture dish 24 h prior to each experiment. Twenty microliters of each DiI-labeled NPs were mixed with 4 μg DNA and then diluted in 1 ml folate-deficient RPMI medium containing 10% serum.

The mixtures were added to the monolayers of KB cells. To determine the selective association of the nanoplex with KB cells, KB cells were incubated with nanoplexes in the presence or absence of 1 mM folic acid. After 1-, 2- and 3-h incubation, the dishes were washed two times with 1 ml PBS (pH 7.4) to remove unbound nanoplex, and the cells were detached with 0.25% trypsin. The cells were centrifuged at 1500 × *g*, and the pellets were lysed with 1 ml of lysis buffer (PBS containing 0.5% Triton X-100). Arbitrary units (a.u.) of DiI fluorescence intensity were then measured using a fluorometer (Hitachi F-4010, Tokyo, Japan) at excitation and emission wavelengths of 550 and 570 nm, respectively. Protein content was estimated using BCA protein assay, and results were expressed as fluorescence (a.u.) per mg/ml of protein lysate.

2.8. Confocal microscopy

KB cells were plated into 35-mm culture dishes. Ten microliters of each NP was mixed with 2 μg DNA and then diluted in 1 ml the complete medium. KB cells were incubated with the mixtures in the presence or absence of 1 mM folic acid for 24 h. After medium removal, cells were washed with PBS and fixed with PBS-buffered 4% formaldehyde solution at room temperature for 1 h, and then washed three times with PBS. Next, the coverslips were put on the dish coated with Aqua Poly/Mount (Polyscience, Warrington, PA, USA) to prevent fading. Examinations were performed with a Radiance 2100 confocal laser scanning microscopy (BioRad, CA, USA). For DiI, maximum excitation was performed by a 543-nm line of internal He–Neon laser, and fluorescence emission was observed with long-pass barrier filter 560DCLP. FITC-labeled DNA was imaged using the 488-nm excitation line of an argon laser, and fluorescence emission was observed with a filter HQ515/30. The contrast level and brightness of the images were adjusted.

2.9. Luciferase assay

The nanoplexes at charge ratios (+/−) of 1/1, 2/1, 3/1, 4/1 or 5/1 of cationic lipid to DNA were formed by addition of NPs to 2 μg DNA with gentle shaking and leaving at room temperature for 10–15 min. For transfection, each nanoplex was diluted in 1 ml complete medium and then incubated for 24 h.

Luciferase expression was measured according to the luciferase assay system. Incubation was terminated by washing the plates three times with cold PBS. Cell lysis solution (Pica gene) was added to the cell monolayers and subjected to one cycle of freezing (−70 °C) and thawing at 37 °C, followed by centrifugation at 15,000 rpm for 5 s. The supernatants were stored at −70 °C until the assays. Aliquots of 20 μl of the supernatants were mixed with 100 μl of luciferase assay system (Pica gene) and counts per second (cps) were measured with a chemoluminometer (Wallac ARVO SX 1420 multilabel counter, Perkin Elmer Life Science, Japan). The protein concentration of the supernatants was determined with BCA reagent using bovine serum albumin as a standard and cps/μg protein was calculated.

2.10. RNA isolation and RT-PCR

Total RNA was isolated from LNCaP and KB cells, respectively, using the NusleoSpin RNA II (Macherey-Nagel, Germany). RNA yield and purity were checked by spectrometric measurement at 260 and 280 nm and RNA electrophoresis, respectively. The first-strand cDNA was synthesized from 5 μg total RNA after denaturation for 5 min at 65 °C by use of 50-pmol random primer, 0.5 mM dNTP and 5 U AMV reverse transcriptase XL (Takara Shuzo, Japan). The reaction was performed at 41 °C for 1 h in a 20-μl volume. For RT-PCR, a 25-μl reaction volume contained the following: 1 μl of synthesized cDNA, 10 pmol of each specific primer pair, 0.25 U Ex Taq DNA polymerase (Takara Shuzo) with a PCR reaction buffer containing 1.5 mM $MgCl_2$ and 0.2 mM of each dNTP. The temperature profile of the PCR amplification consisted of denaturation at 94 °C for 0.5 min, primer annealing temperature at 55 °C for 0.5 min and elongation at 72 °C for 1 min for 30 cycles. PCRs of the housekeeping gene β-actin, FRs (FR-α, -β, -γ) and PSMA were performed at the same cycle run for all samples. The PCR products for FRs, PSMA and β-actin were analyzed by 1.5% agarose gel electrophoresis in Tris–borate–EDTA (TBE) buffer. The products were lighted by ethidium bromide staining.

2.11. Statistical analysis

Statistical significance of the data was evaluated by the Student's *t*-test. A *p*-value of 0.05 or less was considered significant.

3. Results

3.1. Preparation and stability of NPs

Six different cationic NP formulations were prepared as potential nonviral vectors. The components and the compositions of the NPs are presented in Table 1. All formulations consisted of 1 mg/ml DC-Chol as a cationic lipid. NP-T contained 5 mol% Tween 80. NP-0.3PT and NP-1PT contained 5 mol% Tween 80 with 0.3 and 1 mol% PEG_{2000}-DSPE, respectively. In the formulae of NP-0.3FT and NP-1FT for FR-targeting vectors, PEG_{2000}-DSPE in NP-0.3PT and NP-1PT was substituted with 0.3 and 1 mol% f-PEG_{2000}-DSPE, respectively. In NP-1FLT, 1 mol% f-PEG_{5000}-DSPE was used instead of f-PEG_{2000}-DSPE in NP-1FT.

The average sizes and ζ-potentials of each NP were about 100–200 nm and about +50 mV, respectively. Stability of each NP was tested by measuring the change in size with time. No significant change in the average particle size was observed in any NPs for 60 days. All formulae maintained particle size in the presence of electrostatic repulsion and/or steric hindrance of PEG lipid. These findings suggested that NPs prepared in this study were stable in water.

3.2. Characterization of nanoplexes

The physical characteristics of the nanoplexes were investigated. The charge ratio of the cationic NPs to DNA ratio was fixed at 3. The NPs were mixed with DNA and then the change in size was measured. The sizes of each nanoplex slightly increased from 200 to 300 nm (Table 2). The ζ-potential slightly decreased to +30–+40 mV. The size of nanoplex in water slightly increased by 200–350 nm after 24-h incubation (Table 2), and then did not change for up to 72 h (data not shown).

3.3. Stability of nanoplexes in the presence of serum

In serum, there are many anionic materials that would compete with and substitute for DNA in the complex. Such a substitution was assumed to be a major destabilization mechanism for the complex [25,26]. Therefore, we investigated the stability of the nanoplexes (NP-0.3FT, NP-1FT and NP-1FLT) in the presence of 10% or 50% serum. In the presence of 10% serum, the sizes of nanoplexes of NP-0.3PT and NP-1FT increased up to 500 nm, whereas that of NP-1FLT did not significantly change. In the pres-

Table 2
Particle size, stability and ζ-potential of nanoparticles and nanoplexes[a] in the absence and in the presence of serum

Formulation	Nanoparticle[b]			Nanoplex[b]			Nanoplex[c] +10% serum	Nanoplex[c] +50% serum
	Size (nm)		ζ-potential (mV)	Size (nm)		ζ-potential (mV)	Size (nm)	Size (nm)
	0 days	60 days	0 days	0 days	1 days	0 days		
NP-T	146.4	165.8	49.0	221.2	285.4	40.7	nd[d]	nd
NP-0.3PT	114.7	114.7	52.9	200.6	235.8	32.8	nd	nd
NP-1PT	139.3	127.6	53.5	191.6	214.5	40.0	nd	nd
NP-0.3FT	122.0	122.0	51.3	215.6	230.3	37.2	482.9	937.9
NP-1FT	207.4	188.3	46.8	309.1	342.9	33.3	473.0	513.0
NP-1FLT	104.3	126.3	42.3	240.5	248.2	29.6	253.4	303.5

Values represent means ($n=2$).
[a] Charge ratio (+/−) of nanoparticle/DNA=3/1.
[b] In water.
[c] 0 day after mixing of serum.
[d] Not done.

ence of 50% serum, the size of nanoplex of NP-0.3FT increased up to 900 nm, whereas that of NP-1FT and NP-1FLT slightly increased compared with that in the presence of 10% serum. Therefore, the nanoplexes of NP-1FT and NP-1FLT are more likely to maintain its physical integrity in the presence of anionic competitors.

3.4. Optimization of charge ratio in nanoplexes

In the transfection study, we focused on NP-1FT. For optimization of the charge ratio (+/−) of NPs to DNA, luciferase activity was measured in LNCaP cells transfected with NP-1FT at various charge ratios (+/−) in medium with 10% serum. The charge ratio (+/−) of 3/1 showed the highest transfection efficiency. Luciferase activity (cps/μg protein) reached about 1×10^3 at the optimal ratio (Fig. 1).

The size of NP-1FT nanoplex at the charge ratio (+/−) of 3/1 in water was not different compared with that of 1/1 and 5/1. In the presence of 10% serum, the size of NP-1FT nanoplex at the charge ratio (+/−) of 1/1, which had a −37.85 mV, increased to up to 600 nm, but those at the charge ratio (+/−) of 3/1 and 5/1, which had a positive charge, slightly increased up to about 470 nm (data not shown). In the following studies, therefore, we used a charge ratio (+/−) of 3/1 of NPs to DNA.

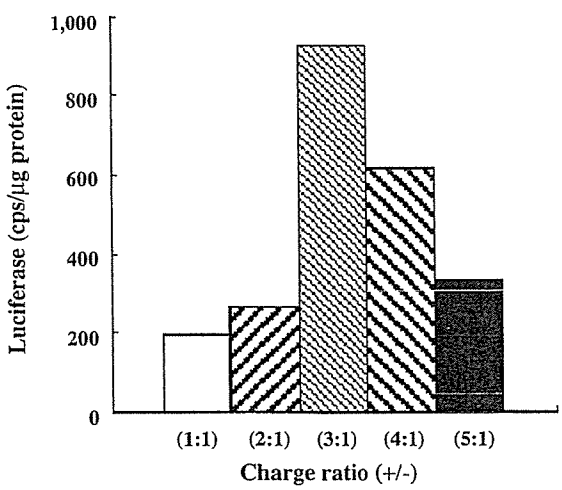

Fig. 1. Gene expressions in LNCaP cells transfected with NP-1FT at various charge ratios (+/−) in medium with 10% serum. LNCaP cells (at a density of 1×10^5 cells/well) were seeded in 6-well plates 24 h before transfection. Nanoplexes were diluted with medium with serum to a final concentration of 2 μg DNA in 1 ml medium per well, and each cell was incubated for 24 h. Each column represents the mean ($n=2$).

3.5. Association of nanoplexes with KB cells

Association of folate-linked NPs with KB cells was compared with that of nonfolate-linked NPs. We decided to use NP-T, -1FT and -1PT for comparison of the association efficiencies. The DiI, a nonexchangeable fluorescent membrane probe, labeled nanoplexes, were prepared from DiI-labeled NPs and incubated with KB cells in the presence of 10% serum. At various times, unbound nanoplexes were removed and bound nanoplexes were measured using DiI. The association of nanoplex of NP-1PT was found to be lower than that of NP-T, possibly due to addition of PEG-DSPE (Fig. 2A). However, that of NP-1FT was found to be restored 1.5-fold higher than that of NP-1PT after 3-h incubation. The presence of 1 mM free folic acid in the medium significantly reduced association with the nanoplex of NP-1FT, but not that of NP-1PT (Fig. 2B). The nanoplex of NP-1FT was taken up about 8% of the initial amount used for transfection at 3-h incubation (data not shown).

3.6. Localization of nanoplexes visualized by confocal microscopy

KB cells were exposed for 24 h to nanoplexes of DiI-labeled NP-1FT, and then fixed in 4% paraformaldehyde and visualized by confocal microscopy. The distribution pattern of DiI red signal on NP-1FT was observed throughout the cells, and the majority of the signal was concentrated in the cell surface (Fig. 3A and B). In contrast, the presence of 1 mM free folic acid in the medium reduced the signal on the cell surface (Fig. 3C and D).

As shown in Fig. 3E and F, LNCaP cells were exposed for 24 h to nanoplexes consisting of DiI-labeled NP-1FT and FITC-labeled plasmid DNA. FITC signal was detected strongly on the cell surface and weakly in cytoplasm (Fig. 3E and F). The colocalization of DiI and FITC signals was detected on the cell surface, suggesting that the plasmid DNA